Edinburgh Research Explorer

Charge order and three-site distortions in the Verwey structure of magnetite

Charge Order And Three-Site Distortions In The Verwey Structure Of Magnetite**

Mark S. Senn,[1] Jon P. Wright[2,]* and J. Paul Attfield[1,]*

[1]Centre for Science at Extreme Conditions and School of Chemistry, University of Edinburgh, West Mains Road, Edinburgh EH9 3JZ, UK.

[2]European Synchrotron Radiation Facility, 6 rue Jules Horowitz, BP 220, 38043 Grenoble Cedex 9, France.

[*]Corresponding authors; J.P.A. e-mail: j.p.attfield@ed.ac.uk; J.P.W e-mail: wright@esrf.fr

Supporting information:
Supplementary Information is linked to the online version of the paper at www.nature.com/nature

Abstract

The mineral magnetite (Fe_3O_4) undergoes a complex structural distortion and becomes electrically insulating at temperatures less than 125 kelvin. Verwey proposed in 1939 that this transition is driven by a charge ordering of Fe^{2+} and Fe^{3+} ions[1], but the ground state of the low-temperature phase has remained contentious[2, 3] because twinning of crystal domains hampers diffraction studies of the structure[4]. Recent powder diffraction refinements[5, 6, 7] and resonant X-ray studies[8, 9, 10, 11, 12] have led to proposals of a variety of charge-ordered and bond-dimerized ground-state models[13, 14, 15, 16, 17, 18, 19]. Here we report the full low-temperature superstructure of magnetite, determined by high-energy x-ray diffraction from an almost single-domain, 40-micrometre grain, and identify the emergent order. The acentric structure is described by a superposition of 168 atomic displacement waves (frozen phonon modes), all with amplitude 0.24 Å. Distortions of the FeO_6 octahedra show that Verwey's hypothesis is correct to a first approximation and that the charge and Fe^{2+} orbital order are consistent with a recent prediction[17]. However, anomalous shortening of some Fe–Fe distances suggests that the localized electrons are distributed over linear three-Fe-site units, which we call 'trimerons'. The charge order and three-site distortions induce substantial off-centre atomic displacements and couple the resulting large electrical polarization to the magnetization. Trimerons may be important quasiparticles in magnetite above the Verwey transition and in other transition metal oxides.

Main text

The cubic spinel type structure of magnetite distorts to a monoclinic superstructure with *Cc* space group symmetry below the $T_V \approx 125$ K Verwey transition[4, 20]. *Cc* domains[21] ~1 μm in size are formed in up to 24 orientations within magnetite crystals, and microtwinning of these domains severely hampers diffraction studies. We have investigated the use of small magnetite grains as potential single-domain crystals for high-energy X-ray structure analysis (Fig. 1). In the smallest and least-twinned grain of many that we investigated, 89% of the scattering was from a single orientation and 11% was from a secondary domain (Fig. 1a). The *Cc* crystal structure was determined using 91,433 symmetry-unique Bragg reflections from this 40-μm grain (see Methods Summary and Methods section in Supplementary Information for details of the structure and derived quantities used below). No further superstructure or lowering of space group symmetry below *Cc* was evident in the diffraction data.
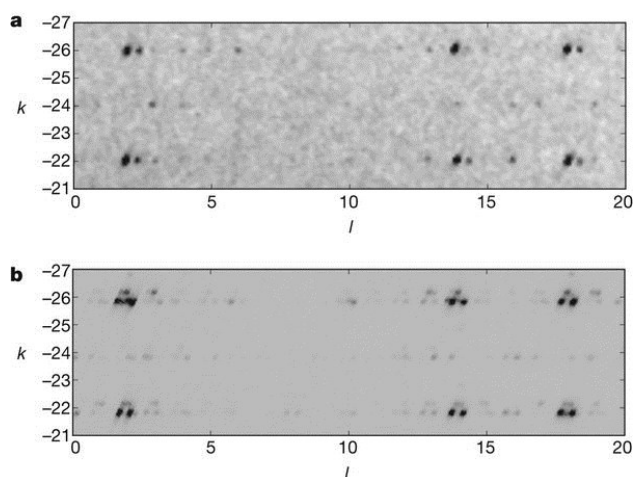


Figure 1. **Reciprocal lattice synchrotron X-ray diffraction intensities for magnetite microcrystal grains at 90 K.** Sections of (*h k l*) intensities in the *h* = 50 plane are shown. **a**, Intensities for an approximately spherical grain of

diameter 40 μm, which was used to determine the crystal structure. The microcrystal is almost single domain; faint spots to the right of the main intensities reveal the secondary twin. **b**, Intensities from an irregular grain of dimension ~100 μm showing multiple twin domains.

The low-temperature *Cc* crystal structure of magnetite has 168 variable (x, y, z) atomic coordinates, of which 166 are independent and two are constrained to fix the cell origin. The coordinates are equivalently described by the same number of amplitudes of frozen displacement waves (phonons), all with values $q < 0.24$ Å, as shown graphically in Fig. 2. Only one of these (an O-site Γ-mode) is present in the high-temperature cubic structure and the remainder all freeze at the Verwey transition. The three largest-amplitude modes have Δ_5 symmetry and are acentric, heralding the large off-centre structural distortions described later, but the smoothly varying distribution of amplitudes shows that many centric and acentric Δ, X and W modes contribute significantly. Hence, the superstructure is not approximated well by a few frozen phonons, and even attempts to describe the important features with up to 100 lattice modes were unsuccessful.
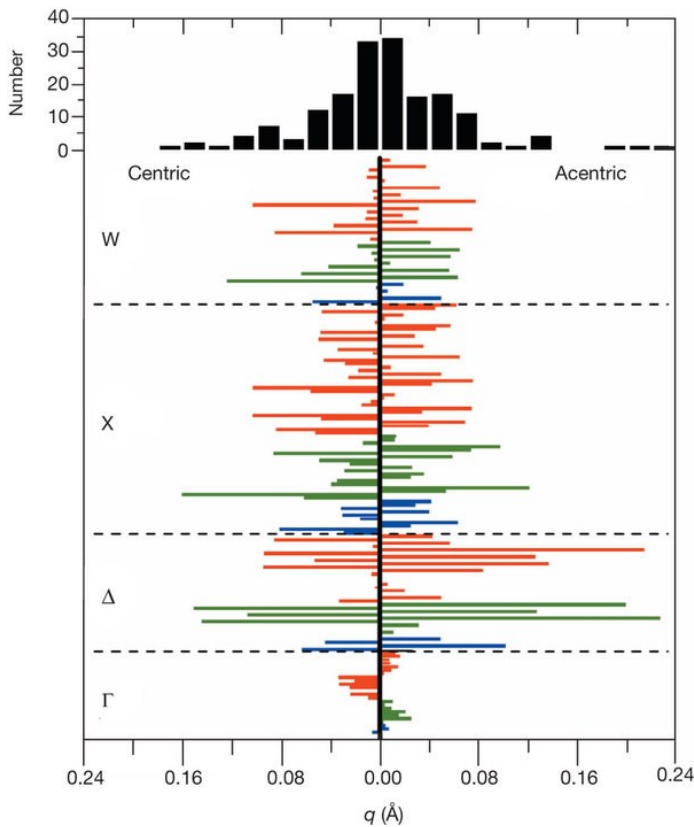
← *Figure 2*. **The 168 displacement amplitudes of the low-temperature *Cc* magnetite structure.** Main panel: centric and acentric mode amplitudes, q, which have estimated standard deviations <0.003 Å. Top panel: distribution of amplitudes. A, B and O atom modes of the cubic $Fd\bar{3}m$ AB$_2$O$_4$ spinel type structure are coloured blue, green and red, respectively. The displacement waves have periodicities corresponding to the Γ (0, 0, 0), Δ (0, 1/2, 0), X (0, 1, 0) and W (1/2, 1, 0) points in the Brillouin zone of the cubic structure. Many acentric and centric Δ, X and W modes involving the B and O sites contribute significantly to the overall superstructure, but the Γ modes are less

Magnetite has an AB$_2$O$_4$ spinel structure in which Fe^{3+} occupies the tetrahedrally coordinated A cation sites, and a 1:1 order of Fe^{2+} and Fe^{3+} is expected over the 16 inequivalent octahedral B sites of the *Cc* superstructure in the Verwey hypothesis. Each B-site FeO$_6$ octahedron has an irregular distortion from which the amplitudes of radial expansion (breathing) local modes (Q_{Rad}) and tetragonal Jahn–Teller (Q_{JT}) local modes were extracted because these are sensitive to charge-ordering and associated orbital-ordering displacements. For Q_{JT} we find a bimodal Verwey-type distribution

(Fig. 3a) in which eight near-zero values are consistent with Fe^{3+}, which is Jahn–Teller inactive as the high-spin $3d^5$ electron configuration is non-degenerate. The other eight Q_{JT} values are negative as expected for $3d^6$ Fe^{2+}, where tetragonal Jahn–Teller compression removes the degeneracy created by the extra electron occupying one of the three t_{2g} symmetry d orbitals (d_{xy}, d_{xz} or d_{yz}). In addition, the plot of Q_{Rad} (the increase in octahedral average Fe–O bond distance) against Q_{JT} shows that the eight Jahn–Teller-distorted B sites are also the eight most expanded, consistent with Fe^{2+}, and that the eight undistorted sites are the least expanded, as expected for Fe^{3+}. The bimodal distribution of tetragonal distortions and their correlation with the radial amplitudes demonstrate experimentally that Verwey's Fe^{2+}–Fe^{3+} ordering hypothesis is correct to a useful first approximation. However, the distribution of Q_{Rad} and equivalent bond valence sum (BVS) estimates of formal Fe charge (Fig. 3a) does not seem bimodal, indicating the more complex electronic order described later.
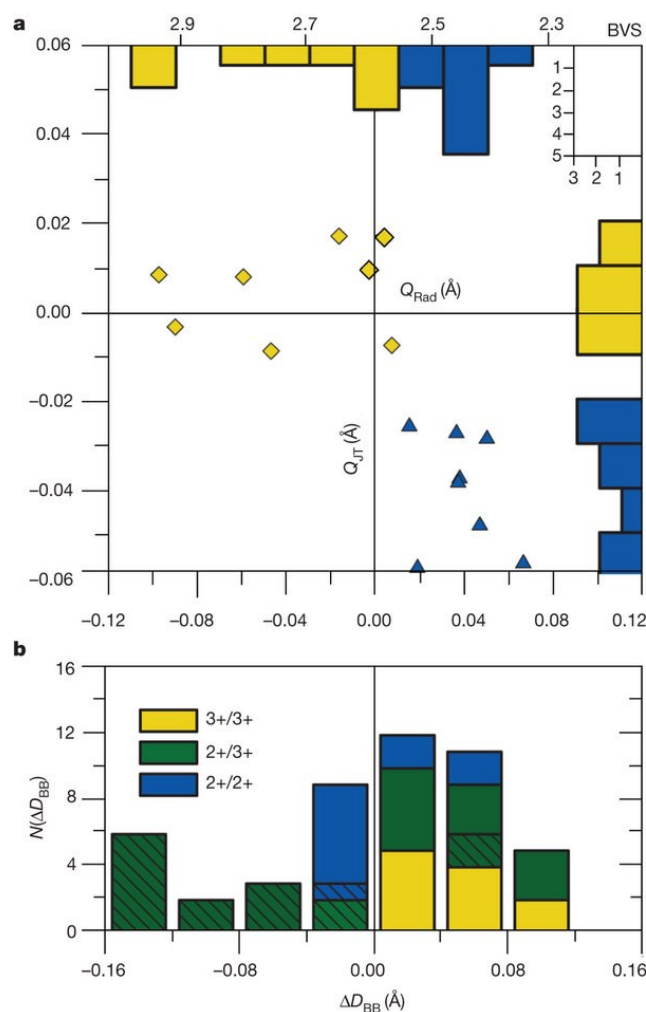
Figure 3. **Local distortion distributions that reveal electronic order in the low-temperature magnetite structure.**
(a) Plot of local distortions for the 16 distinct FeO_6 octahedra. Q_{Rad} and Q_{JT} are the amplitudes of the radial (breathing) and tetragonal Jahn–Teller distortions. Their estimated standard deviations of <0.002 Å are smaller than the symbols shown. Q_{Rad} is the difference between the average Fe–O bond distance in an FeO_6 octahedron and the average over all octahedra. The points fall into two groups describing characteristic local distortions for Fe^{2+} and Fe^{3+} (blue and yellow bars and symbols, respectively). The distributions of the two modes (inside top and right edges of plot, with scales top right) show that there is bimodal segregation of the Q_{JT} amplitudes but that the Q_{Rad} dispersion is more continuous. BVS estimates of formal Fe charge are shown above the Q_{Rad} distribution. **(b),** Distribution of the 48 distinct Fe–Fe

distances between neighbouring B sites, relative to the average D_{BB} (= 2.967 Å), coloured according to the Fe charge states. The 16 distances from the eight Fe^{2+} sites to their two neighbours perpendicular to the local orbital ordering axis (Fe^{3+} in 15 cases and Fe^{2+} once) are hatched. The anomalous shortening of most of these distances indicates the linear three-site (trimeron) distortions as shown in Fig. 4c.

The average BVS formal oxidation states for the eight Fe^{2+}- and Fe^{3+}-like B sites in the *Cc*magnetite structure are 2.47 and 2.75, respectively, consistent with an earlier partial refinement[5, 6]and structural results for other charge-ordered transition metal oxides[22]. The Fe^{2+}–Fe^{3+}arrangement (Fig. 4a) differs from the original prediction of Verwey[23], but the charge and Fe^{2+}orbital ordering (Fig. 4b) are in agreement with a recent model based on electronic structure calculations[17]. The arrangement is close to a centric structure in which the Fe^{2+} states form chains of corner-linked $(Fe^{2+})_3$ triangles, but with a neighbouring Fe^{2+}–Fe^{3+} pair exchanged at every fourth triangle as shown (Fig. 4a). Anderson's condition[24] that each tetrahedron of four neighbouring B sites should contain two Fe^{2+} ions is only satisfied in a quarter of the tetrahedra. The complexity of the charge and orbital ordering may be explained in part by the distribution of Jahn–Teller distortions. The octahedral compressions of the 16 Fe^{2+} sites in the basic cell act parallel to the *a*, *b*, and *c* axes of the high-temperature cubic lattice in a 5:5:6 ratio that minimizes strain in the highly connected spinel lattice. More-symmetric charge and orbital orderings tend to have less equal ratios. The small anisotropy arising from excess distortion in the *c* direction may account for the change in magnetic easy-axis from cubic [111] to [001] at temperatures less thanT_V.
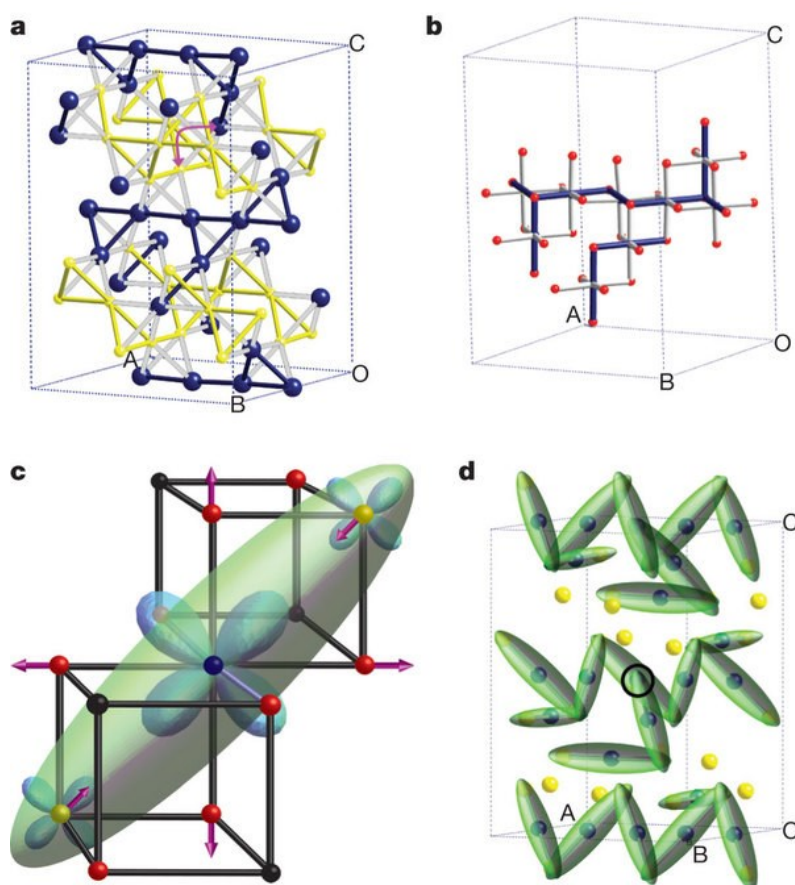
Figure 4. **Charge, orbital and trimeron order in the low-temperature magnetite structure. (a)** Distribution of Fe^{2+} and Fe^{3+} states (blue and yellow spheres, respectively) in the first-approximation Verwey-type model, shown in

the $\sqrt{2}a \times \sqrt{2}a \times 2a$ Cc supercell (a is the high-temperature cubic-cell parameter). Nearest-neighbour Fe^{2+}–Fe^{2+} connections (blue lines) describe irregular chains, parallel to the a axis, derived from a more symmetric, centric arrangement of corner-linked triangles by exchange of Fe^{2+}–Fe^{3+} pairs (one pair indicated). **(b)** Jahn–Teller distortions arising from orbital order within a single Fe^{2+} chain shown as long and short bonds (grey and blue lines, respectively) to oxygen atoms (red spheres). **(c)** Coupled distribution of a minority-spin electron (with approximate atomic populations indicated by the sizes of blue t_{2g} orbitals) and associated atomic displacements (purple arrows) within a linear three-Fe-site (trimeron) unit. Orbital order at the central Fe^{2+} site (blue) localizes the minority-spin electron in one of the t_{2g} orbitals and elongates the four Fe–O bonds perpendicular to the local Jahn–Teller axis. Weak bonding interactions transfer minority-spin density into coplanar t_{2g} orbitals at two neighbouring B sites (shown as yellow Fe^{3+}) and shorten the Fe–Fe distances. The minority-spin electron density is approximated by a scalene ellipsoid encompassing the three Fe sites. Other B-site Fe^{2+} or Fe^{3+} neighbours (black spheres) do not participate. **(d)** Trimeron distribution in the low-temperature magnetite structure, following the experimentally observed distortions, with Fe^{2+} and Fe^{3+} states shown as blue and yellow spheres, respectively, and trimeron ellipsoids as in **c**. The trimerons are mainly end-linked through Fe^{3+} ions, but one trimeron is terminated by an Fe^{2+} ion (circled). Some Fe^{3+} sites do not participate in any trimerons.

Edge sharing of FeO_6 octahedra allows direct B–B electronic interactions within linear chains that extend in six directions. The nearest-neighbour B–B distances, D_{BB}, are all equivalent in the cubic magnetite structure, but $D_{BB}(Fe^{2+}$–$Fe^{3+})$, the nearest-neighbour Fe^{2+}–Fe^{3+} distance, in particular shows a wide distribution in the Verwey phase (Fig. 3b). Electrostatic repulsions tend to disperse the distance values such that $D_{BB}(Fe^{2+}$–$Fe^{2+}) < D_{BB}(Fe^{2+}$–$Fe^{3+}) < D_{BB}(Fe^{3+}$–$Fe^{3+})$, so the observed tail of anomalously short Fe^{2+}–Fe^{3+} distances is not expected in a Verwey model and indicates magnetically driven B–B bonding by the additional t_{2g} electrons. (The five parallel unpaired d-electron spins at all B sites are ferromagnetically ordered below the Curie temperature (858 K), so only the additional electron from each $3d^6$ Fe^{2+} state has an opposed, minority, spin and may be delocalized between B sites through bonding.) Chains of alternating short and long B–B distances are predicted in bond-dimerized models[13, 16,19], but are not observed in our structure. Instead, the two B–B distances perpendicular to the local orbital-ordering axis at each of the eight Fe^{2+} positions both tend to be shortened: this is the case for 14 of these 16 distances (Fig. 3b, hatched). This suggests that minority-spin t_{2g} electron density is significantly delocalized from an Fe^{2+} donor onto two adjacent B-site acceptors, which are usually Fe^{3+} sites. This single charge, delocalized over three B sites with associated displacements of the two acceptor B sites and surrounding oxygen atoms (Fig. 4c), corresponds to a highly structured small polaron that may be described as a 'trimeron', by analogy with dimeron quasiparticles in $La_{1−x}Ca_xMnO_3$ (ref. 25). Fifteen of the 16 trimeron acceptor sites are Fe^{3+} ions, but one Fe^{2+} (Fig. 4d, circled) accepts into a t_{2g} orbital that is orthogonal to its own trimeron. Trimeron distortions are intrinsically symmetric (having $D_{BB} = 2.832$ and 2.848 Å in the most regular environment of the Cc structure, where $D_{BB} = 2.967$ Å on average), but asymmetric connectivity leads to off-centre distortions and long B–B bonds in 2 of 16 cases.

The linear three-site (trimeron) distortions (Fig. 4d) significantly perturb charge order in the Cc magnetite structure and couple the magnetism to the complex overall distortion. Only two B ions are available per minority-spin electron, so trimeron units are constrained to share sites. End-sharing connections with angles of 60°, 120° and 180° are possible, but 180° linkages are apparently avoided to maximize charge transfer because two or three different t_{2g} orbitals are

used by an Fe^{3+} ion participating in two or three trimerons. This is analogous to the formation of two or three short *cis*-bonds in some d^0 transition metal oxides and oxynitrides[26], and creates off-centre Fe^{3+} displacements that contribute strongly to the acentric lattice modes and electric polarization. High connectivity seems favourable because four of the eight Fe^{3+} sites participate in the maximum of three trimerons. The orderings of linear three-site, one-electron units along the infinite B chains correspond to charge density waves with wavevector magnitude $q_c = 1/N$ for a repeat sequence of one trimeron for every N B sites. The structural average is $q_c = 1/6$ but only chains with $q_c = 0$, $1/8$ and $1/4$ are present, in a 1:6:5 ratio. The unique $q_c = 0$ chain contains only Fe^{2+} ions (Fig. 4a, b) but their three-site distortions are always within other chains.

The linear three-site distortions we attribute to trimerons also account for the non-Verwey distribution of radial amplitudes (Q_{Rad}) and BVS values for the B-site FeO_6 octahedra (Fig. 3a). Each Fe^{2+} ion donates minority-spin t_{2g} electron density to two B-site acceptors within a trimeron (Fig. 4c), so the eight Fe^{2+}-like sites have a narrow Q_{Rad} distribution and BVS ≈ 2.4. However, Fe^{3+} ions are acceptors in varying numbers of trimerons. Two Fe^{3+} sites do not participate in any trimerons and so have the two lowest Q_{Rad} values and the highest B-site BVS values, ~3.0 (Fig. 3a). The other six Fe^{3+} sites are acceptors for one to three trimerons and thus have a spread of higher Q_{Rad} values and lower valences with BVS ≈ 2.6–2.8. Charge transfer within trimerons tends to equalize the electron density across B sites: in the limit of maximum donor-to-acceptor transfers (of $0.2e$, where e is the electron charge), an Fe^{3+} ion participating in three trimerons has the same formal charge, $+2.4e$, as the Fe^{2+} donor sites. However, the two states are still distinguished by their minority-spin t_{2g} distributions, as the former site has populations $d_{xy}^{0.2}d_{xz}^{0.2}d_{yz}^{0.2}$ that preserve the high symmetry of Fe^{3+}, whereas the latter has a distribution such as $d_{xy}^{0.6}d_{xz}^{0}d_{yz}^{0}$, retaining the orbital order of Fe^{2+}. This justifies the use of formal valence states to describe charge-ordered structures even when the apparent charge separations are small, as here in magnetite.

The discovery of multiferroism in charge-ordered $LuFe_2O_4$ (ref. 27) has led to recent interest in the coupling of magnetism and the ferroelectric polarization expected in the acentric Cc magnetite superstructure[16, 17]. Measured electric polarization values of $P \approx 0.05$ C m^{-2} for magnetite crystals and thin films agree with estimates from previous structural models[17], but an Fe^{2+}–Fe^{3+}–O^{2-} point-charge calculation for our structure gives a polarization larger by an order of magnitude ($P_a = 0.118$ C m^{-2}, $P_c = 0.405$ C m^{-2}; $P = 0.422$ C m^{-2}; where P_a and P_c are the respective magnitudes of the polarization vector components parallel to the crystallographic a and c axes and P is the magnitude of the resultant polarisation vector). The same calculation with average $Fe^{2.5+}$ B-site charges gives similar results ($P_a = 0.080$ C m^{-2}, $P_c = 0.346$ C m^{-2}; $P = 0.355$ C m^{-2}), showing that atomic displacements resulting from charge order and three-site distortions are responsible for most of the polarization, with exchange of Fe^{2+}–Fe^{3+} pairs (Fig. 4a) contributing only 16% of the total. The large P_c component, parallel to the magnetic easy axis, shows that a substantial magnetoelectric coupling is expected in single magnetite domains.

Lattice effects are significant in the cubic phase of magnetite as diffuse scattering is observed above the Verwey transition,[12, 28] and the electrical conductivity rises continuously to a maximum at ~3T_V. Hence, trimeron fluctuations may be significant quasiparticles in the cubic phase. The expected entropy change at the Verwey transition is conventionally assumed to be $R\ln4 = 1.4R$ (R is the molar gas constant) for full disorder of Fe^{2+}/Fe^{3+} charges, but our structure shows that this change should be $R\ln12 = 2.5R$ for additional randomisation of the triply-degenerate Fe^{2+} orbital states. Hence the observed entropy change of ~0.7R corresponds to only 30% of the possible disorder at T_V.[29]

Previous estimates have used Anderson or other charge configurations within tetrahedra of four B sites, but trimeron-based models may provide alternative predictions. An approximate calculation based on the above local connectivity of Fe^{3+} sites reduces the predicted transition entropy from 2.5R to 2.1R (or from 1.4R to 1.0R if orbital states are neglected) – these estimates are still greater than above the observed value and suggest that trimeron or other correlations persist above T_V.

In conclusion, we have determined the low temperature structure of magnetite to high experimental precision from high energy x-ray structure analysis of a small, almost single-domain, magnetite grain. Many frozen lattice modes contribute to the *Cc* superstructure including substantial acentric amplitudes from which a large electrical polarisation is predicted. Verwey's charge ordering hypothesis is correct to a useful first approximation, but analysis of the Fe-Fe distances indicates that the minority spin Fe^{2+} electrons are delocalised over linear three-site (trimeron) units. Selforganisation of the charge and orbital states couples the spin order of this eponymous magnetic material to the complex Verwey distortion. Trimerons may be significant quasiparticles above the Verwey transition and may also be relevant to other transition metal oxides such as superconducting $LiTi_2O_4$ spinel. Finally, we note that a full *ab initio* simulation of the low-temperature magnetite structure starting from calculations on the cubic state presents a future challenge to improve understanding of the Verwey phase, now that the experimental structure has been determined.

Methods Summary

Grains from a highly stoichiometric powder used in previous studies[5, 6, 8] were placed in a 100-μm, focused monochromatic beam (wavelength, 0.16653(1) Å; estimated standard deviation shown in parenthesis) on the ID11 diffractometer at ESRF, Grenoble. Multiple scattering and extinction problems were reduced by using small crystallites and a high X-ray energy (74 keV), which also gave access to an abundance of diffraction peaks at very high momentum transfer and reduced absorption effects. Crystals were aligned and de-twinned using a permanent magnet (producing a field of approximately 0.1 T at the sample), and were verified as being cubic single domains at 130 K before cooling through the Verwey transition to 90 K.

The grain used for structure determination was approximately spherical with diameter ~40 μm. We used ω-scans with varying exposure times to increase the dynamic range of the data from the charge-coupled-device detector (Frelon2K camera) and these were performed at azimuthal anglesφ and $\varphi + 180°$ to improve data redundancy and test for multiple scattering. Reciprocal lattice sections (Fig. 1a) were reconstructed using local software. Small-box integrations were used to identify the orientation of the two observed domains, and large-box integration was performed to encompass intensity from both domains and allow structure refinement as a pseudo-merohedral twin.

2,000 starting models were generated by applying random atomic displacements to the high-temperature structure and were optimized by least-squares refinement. A global minimum at residual $R[F^2 > 4\sigma] = 4.99\%$ (where F and σ are the observed magnitude and standard deviation of a structure factor) was observed most frequently (292 times), in addition to local refinement minima ($R[F^2 > 4\sigma] \geq 5.88\%$). The final refinement of the global minimum model used independent anisotropic thermal parameters for all atoms and all data to a resolution of $d \geq 0.3$ Å, giving R values$R[F^2 > 4\sigma] = 3.40\%$, $R[F^2] = 5.18\%$ and weighted residual $wR_2 = 6.96\%$. Full crystallographic information and details of the analysis software are given in Supplementary Information.

References

[1] Verwey, E. J. W. Electronic conduction of magnetite (Fe_3O_4) and its transition point at low temperatures. *Nature* **144**, 327–328 (1939).

[2] Walz, F. The Verwey transition: a topical review. *J. Phys. Condens. Matter* **14**, R285–R340(2002).

[3] Coey, M. Condensed-matter physics: charge-ordering in oxides. *Nature* **430**, 155–157 (2004).

[4] Iizumi, M. *et al.* Structure of magnetite (Fe_3O_4) below the Verwey transition-temperature. *Acta Crystallogr. B* **38**, 2121–2133 (1982).

[5] Wright, J. P., Attfield, J. P. & Radaelli, P. G. Long range charge ordering in magnetite below the Verwey transition. *Phys. Rev. Lett.* **87**, 266401 (2001).

[6] Wright, J. P., Attfield, J. P. & Radaelli, P. G. Charge ordered structure of magnetite Fe_3O_4below the Verwey transition. *Phys. Rev. B* **66**, 214422 (2002).

[7] Blasco, J., Garcia, J. & Subias, G. Structural transformation in magnetite below the Verwey transition. *Phys. Rev. B* **83**, 104105 (2011).

[8] Goff, R. J., Wright, J. P., Attfield, J. P. & Radaelli, P. G. Resonant X-ray diffraction study of the charge ordering in magnetite. *J. Phys. Condens. Matter* **17**, 7633–7642 (2005).

[9] Nazarenko, E. *et al.* Resonant X-ray diffraction studies on the charge ordering in magnetite.*Phys. Rev. Lett.* **97**, 056403 (2006).

[10] Joly, Y. *et al.* Low-temperature structure of magnetite studied using resonant X-ray scattering.*Phys. Rev. B* **78**, 134110 (2008).

[11] Bland, S. R. *et al.* Full polarization analysis of resonant superlattice and forbidden X-ray reflections in magnetite. *J. Phys. Condens. Matter* **21**, 485601 (2009).

[12] Lorenzo, J. E. *et al.* Charge and orbital correlations at and above the Verwey phase transition in magnetite. *Phys. Rev. Lett.* **101**, 226401 (2008).

[13] Seo, H., Ogata, M. & Fukuyama, H. Aspects of the Verwey transition in magnetite. *Phys. Rev. B* **65**, 085107 (2002).

[14] Jeng, H. T., Guo, G. Y. & Huang, D. J. Charge-orbital ordering and Verwey transition in magnetite. *Phys. Rev. Lett.* **93**, 156403 (2004).

[15] Jeng, H. T., Guo, G. Y. & Huang, D. J. Charge-orbital ordering in low-temperature structures of magnetite: GGA+U investigations. *Phys. Rev. B* **74**, 195115 (2006).

[16] van den Brink, J. & Khomskii, D. I. Multiferroicity due to charge ordering. *J. Phys. Condens. Matter* **20**, 434217 (2008).

[17] Yamauchi, K., Fukushima, T. & Picozzi, S. Ferroelectricity in multiferroic magnetite Fe_3O_4 driven by noncentrosymmetric Fe^{2+}/Fe^{3+} charge-ordering: first-principles study. *Phys. Rev. B* **79**, 212404 (2009).

[18] Zhou, F. & Ceder, G. First-principles determination of charge and orbital interactions in Fe_3O_4. *Phys. Rev. B* **81**, 205113 (2010).

[19] Fukushima, T., Yamauchi, K. & Picozzi, S. Ab initio investigations of Fe^{2+}/Fe^{3+} bond dimerization and ferroelectricity induced by intermediate site/bond-centered charge ordering in magnetite. *J. Phys. Soc. Jpn* **80**, 014709 (2011).

[20] Yoshida, J. & Iida, S. X-ray-diffraction study on low-temperature phase of magnetite. *J. Phys. Soc. Jpn.* **42**, 230–237 (1977).

[21] Kasama, T., Church, N. S., Feinberg, J. M., Dunin-Borkowski, R. E. & Harrison, R. J. Direct observation of ferrimagnetic/ferroelastic domain interactions in magnetite below the Verwey transition. *Earth Planet. Sci. Lett.* **297**, 10–17 (2010).

[22] Attfield, J. P. Charge ordering in transition metal oxides. *Solid State Sci.* **8**, 861–867 (2006).

[23] Verwey, E. J. W. & Heilmann, E. L. Physical properties and cation arrangement of oxides with spinel structures. 1. Cation arrangement in spinels. *J. Chem. Phys.* **15**, 174–180 (1947).

[24] Anderson, P. W. Ordering and antiferromagnetism in ferrites. *Phys. Rev.* **102**, 1008–1013 (1956).

[25] Downward, L. *et al.* Universal relationship between magnetization and changes in the local structure of $La_{1-x}Ca_xMnO_3$: evidence for magnetic dimers. *Phys. Rev. Lett.* **95**, 106401 (2005).

[26] Yang, M. H. *et al.* Anion order in perovskite oxynitrides. *Nat. Chem.* **3**, 47–52 (2011).

[27] Ikeda, N. *et al.* Ferroelectricity from iron valence ordering in the charge-frustrated system $LuFe_2O_4$. *Nature* **436**, 1136–1138 (2005).

[28] Yamada, Y., Wakabayashi, N. & Nicklow, R. M. Neutron diffuse-scattering in magnetite due to molecular polarons. *Phys. Rev. B* **21**, 4642–4648 (1980).

[29] Shepherd, J. P., Koenitzer, J. W., Aragon, R., Sandberg, C. J. & Honig, J. M. Heat-capacity studies on single-crystal annealed Fe_3O_4. *Phys. Rev. B* **31**, 1107–1113 (1985).